Experimental investigations of potassium chemistry in premixed flames

Leffler, Tomas; Brackmann, Christian; Weng, Wubin; Gao, Qiang; Aldén, Marcus; Li, Zhongshan

Published in:
Fuel

DOI:
10.1016/j.fuel.2017.05.013

2017

Document Version:
Publisher's PDF, also known as Version of record

Fuel 203 (2017) 802–810

Contents lists available at ScienceDirect

Fuel

journal homepage: www.elsevier.com/locate/fuel

Full length article

Experimental investigations of potassium chemistry in premixed flames

Tomas Leffler [a,b], Christian Brackmann [a,*], Wubin Weng [a], Qiang Gao [a], Marcus Aldén [a], Zhongshan Li [a]

[a] Division of Combustion Physics, Lund University, Box 118, SE-221 00 Lund, Sweden
[b] R&D, Strategic Development, Vattenfall AB, SE-814 26 Älvkarleby, Sweden

HIGHLIGHTS

- Optical measurements of alkali species in premixed laminar flames seeded with KCl.
- Quantitative species concentrations have been evaluated from experimental data.
- Measurements show good agreement with predictions of a chemical mechanism.

GRAPHICAL ABSTRACT

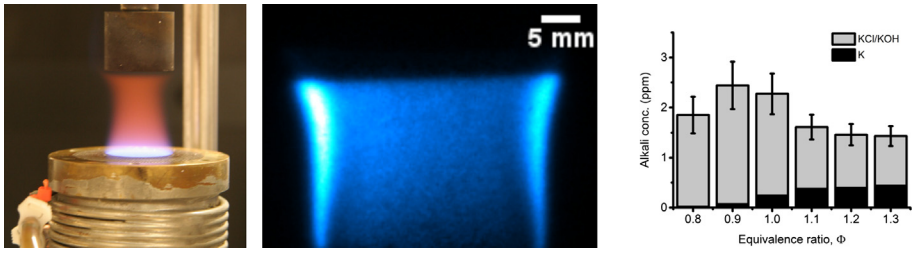

ARTICLE INFO

Article history:
Received 21 February 2017
Received in revised form 3 May 2017
Accepted 4 May 2017
Available online 16 May 2017

Keywords:
Combustion
Alkali formation
Optical diagnostics

ABSTRACT

Quantitative potassium species concentrations have been measured in alkali-seeded premixed methane-air flames of different stoichiometry. Potassium chloride (KCl) and hydroxide (KOH) were measured by broadband UV absorption spectroscopy and laser-induced photofragmentation fluorescence, while atomic potassium was measured using tuneable diode-laser spectroscopy. In addition, laser Rayleigh scattering was employed for temperature measurements. Investigations were made for different alkali-seeding levels and chlorine loads resulting in KCl/KOH concentrations up to ~30 ppm and concentrations of K atoms at ppm levels. Experimental results were compared with predictions from a chemical mechanism used in a homogenous reactor model. The observed trends, decrease in KCl and KOH concentrations and increase in K-atom concentrations with flame equivalence ratio, were well reproduced in simulations and are compared with results reported in literature. In addition, possibilities using the experimental methods for further investigations of alkali-related combustion phenomena and detailed model validation of alkali chemistry are discussed.

1. Introduction

Increased attention to limited fossil fuel resources and the impact of combustion emissions on climate, environment, and health continuously promotes efforts to implement sustainable concepts for future energy supply. Even though solar- and wind based systems have been introduced, combustion remains a major supply of energy worldwide, which has motivated use of renewable biomass fuels [1]. While combustion of such fuels is considered to produce no net CO_2 and thereby have reduced impact on global warming, it still has substantial impact on the environment [1]. Moreover, the chemical composition of biomass fuels introduces new challenges to achieve combustion with minimum wear of power plant units and minimum pollutant emissions [2].

Biomass from wood or crops contains alkali species (mainly potassium) as well as chlorine and sulfur [3–6], and formation of alkali compounds during combustion is of high practical importance since corrosive alkali chlorides cause severe problems in boilers and furnaces [2,7]. In addition, deposits formed on surfaces such as heater and steam tubes contribute to problems with fouling and slagging [8]. Thus, detailed knowledge on alkali release and formation processes during combustion is crucial for efficient uti-

* Corresponding author.
E-mail address: christian.brackmann@forbrf.lth.se (C. Brackmann).

http://dx.doi.org/10.1016/j.fuel.2017.05.013
0016-2361/

lization of biomass fuel while also minimizing problems during power plant operation.

Trace-level species, such as alkali and chlorine [3], in the fuel are many times neglected in combustion models, but have nevertheless been found to have rather strong impact on the overall combustion process, affecting the fuel oxidation process as well as formation of NO_x [9]. According to the discussion in the review by Glarborg [9], this has mainly been attributed to the ability of these reactive species to participate in chain-branching or chain-terminating chemical reactions resulting in production or consumption of flame radicals such as H and OH. In combustion chemistry, potassium atoms are reported to consume flame radicals such as O and H forming potassium hydroxide (KOH), which in turn establishes rapid equilibrium with potassium chloride (KCl) [9]. The combustion chemistry of potassium and chlorine is also coupled to that of sulfur via the ability to transform potassium chloride to less harmful alkali sulfates [10]. Thus, in addition to understanding pollutant formation of alkali species, knowledge on their impact on the overall combustion process and coupling with each other via the flame radical pool is necessary for development of models for biomass fuel combustion. Such combustion can be carried out under a variety of conditions, including co-combustion with coal [11], flameless combustion at very lean conditions [12], or oxy-fuel combustion in an atmosphere augmented with CO_2 [13]. Comprehensive combustion models are therefore required for predictions of relevant quantities such as species concentrations.

Detailed studies of alkali chemistry in flames allow for development of chemical mechanisms, which enable predictions of alkali formation under different combustion conditions. Experimental data acquired under well-defined conditions are crucial for further development and validation of such mechanisms. For example, a study including experiments as well as kinetic modelling of sodium-species in hydrogen flames has been presented by Hynes et al. [14]. For potassium, early investigations have included studies on its effect on flame inhibition [15] but also potassium kinetics in premixed methane flames [16]. A rather recent study was made to investigate the effect of sulfur addition on potassium-species formation [17]. In addition to studies of gaseous fuels, detailed characterization of potassium release has also been carried out for single particles of coal [18] and biomass [19].

According to the work presented by Slack et al. [16], potassium participates in chemical reactions involving O_2, atomic hydrogen, the hydroxyl radical (OH), and water when introduced in a flame. The potassium species involved in these reactions are atoms, potassium hydroxide, potassium oxide (KO), and potassium dioxide (KO_2). Moreover, fuel-rich combustion conditions result in increased formation of atomic potassium via reactions between potassium hydroxide and hydrogen atoms. Conversely the levels of potassium hydroxide are increasing at lean conditions favoured by the availability of oxygen and water. If potassium is introduced together with chlorine in a flame, additional reactions will be included involving species such as atomic chlorine, hydrogen chloride, and potassium chloride [20]. Corresponding investigations of combustion in flames burning hydrogen or propane with sodium and chlorine added, show similar trends with increasing levels of alkali atoms at higher equivalence ratios while chloride and hydroxide concentrations decrease [20].

This paper presents potassium species concentration measurements in alkali-seeded premixed methane-air flames. The methods employed for species concentrations measurements include broadband UV absorption spectroscopy [21], laser-induced photofragmentation fluorescence [21,22], and diode-laser absorption spectroscopy [21,23]. Multiple optical diagnostic techniques have been employed for separate measurements in this work due to the large dynamic range of concentrations encountered in the investigated flames. However, combined measurements of K atoms, KOH, and KCl have been presented previously by Sorvajärvi et al. [24]. Measured potassium species concentrations are compared and the dependence on flame equivalence ratio is analysed and discussed in terms of results previously reported in literature. The obtained results can be further employed for future validation and refinement of alkali flame chemistry models.

2. Experimental

2.1. Optical diagnostics

Laser-induced photofragmentation fluorescence (LIPF) measurements were made using an ArF Excimer laser (Compex 102, Lambda Physik), which provided pulses at a wavelength of 193 nm with 25 ns pulse duration and output pulse energy of 50 mJ. The laser beam was focused using cylindrical lenses of focal lengths f = 1000 mm and f = 500 mm, which combined with an arrangement of razorblades resulted in a 20 mm vertical sheet. The photofragmentation-induced fluorescence signal was detected with an intensified CCD camera (PI-MAX I, Princeton Instruments) equipped with an f = 50 mm objective (Nikkor f/1.4). A bandpass filter centred at 766 nm (50 mm dia., OD 4, FWHM 10 nm, Edmund Optics) was used for suppression of scattered laser radiation.

The evaluation of alkali species concentrations from the photofragmentation fluorescence signal has been described in detail in a previous publication [25]. In brief, the signal, F, is given by Eq. (1)

$$F = \frac{\Omega}{4\pi} l \varepsilon_F A \frac{A_{fi}}{A_{fi}+Q} TN \quad (1)$$

where Ω is the detection solid angle, l the probe volume length, ε_F the detection efficiency for the fluorescence signal, and A is the probe volume cross section area. The fluorescence quantum yield is given by $\frac{A_{fi}}{A_{fi}+Q}$ where A_{fi} is the Einstein coefficient for spontaneous emission and Q the collisional quenching rate.

The transmission factor T accounts for fluorescence losses due to absorption, so-called trapping, which in this case is generated by atomic potassium formed in the flame chemistry. To determine this factor, spectra of the potassium D_1 line at 769.9 nm were obtained from tuneable diode laser absorption measurements, discussed in the following. The spectral line was fitted by a Voigt profile with a Gaussian width of 0.11 cm^{-1} and a Lorenzian width of 0.05 cm^{-1}. An average integrated absorption cross section for the two 4^2P transitions was determined from spectroscopic data in literature [26] to $8.36 \cdot 10^{-6}$ cm^2 s^{-1} and the peak absorption cross section for the fitted lineshape was then calculated to $1.6 \cdot 10^{-11}$ cm^2. Using this quantity, the transmission factor T was calculated according to the Beer-Lambert absorption law under optically thick conditions [27,28] described more in detail in the Supplementary Material. The calculation requires the absorption cross section, given above, the concentration of K atoms, and the absorption path length as input parameters. Values of K-atom concentrations were determined from data of tuneable diode laser absorption measurements, while a path length of 1 cm was estimated for the passage to the detector in the central region of the flame.

Coefficients for spontaneous emission and data on collisional quenching have been obtained from literature [26,29]. The beam cross section area A, is determined by dimensions of the of the focused laser sheet, which had a height of 20 mm and a width estimated to 200 μm. The solid angle and detection efficiency can be retrieved by calibration using the Rayleigh scattering signal.

The quantity N in Eq. (1) is the concentration of K atoms generated in the excited 4^2P states by photofragmentation of potassium compounds and the concentration of these compounds, N_{KCl}, is

related to the evaluated concentration of K atoms according to Eq. (2)

$$N = N_{KCl}\Phi\left(1 - e^{\frac{-\sigma E}{h\nu_{laser}A}}\right) \quad (2)$$

The factor Φ is the yield of photofragments generated from the parent species and is equal to 1 since dissociation of one KCl/KOH molecule results in creation of one K (4^2P) atom. In the exponential term σ is the absorption cross section, E the laser pulse energy, h Planck's constant, and ν_{laser} the laser frequency.

Rayleigh scattering measurements were made using the 532 nm second harmonic of a Nd:YAG laser (Brilliant B, Quantel) with a pulse duration of 7 ns and a pulse energy of 120 mJ. The 532 nm beam was aligned into the beam path and shaped into a laser sheet of 10 mm width using cylindrical lenses of focal lengths f = −40 mm, f = 200 mm, and f = 500 mm. A half-wave plate positioned in the beam path was adjusted to achieve vertical polarization for optimal Rayleigh scattering. The Rayleigh scattering signal measured at ambient conditions provides the detection solid angle, Ω, and the probe volume length, l, in the concentration evaluation using Eq. (1). In addition, Rayleigh scattering can be utilized for flame temperature measurements by comparison of signals measured in flame and at ambient conditions, taking differences in cross sections into account. Using Rayleigh scattering cross-section data compiled by Zetterberg [30] and species concentrations determined from chemical equilibrium calculations, the Rayleigh scattering cross sections of the product gas in the post-flame region of the investigated flames were found to be typically 10% higher than that of ambient air.

Broadband UV absorption measurements of KCl were made using a UV light source (L1314, Hamamatsu). The light was emitted through an aperture and collimated using a 90° off-axis parabolic mirror with a reflective focal length of f = 150 mm (diameter 50 mm, Thorlabs). The collimated UV light beam subsequently passed through another aperture and a plano-convex focusing quartz lens of focal length f = 150 mm. The UV beam was guided in six passages across the burner through the flame using UV-enhanced aluminium mirrors (diameter 25.4 mm, Thorlabs) and then collected in an UV-enhanced collimator (250–450 nm, diameter 12 mm beam, SMA, Thorlabs). This arrangement gave a total absorption path length of 138 mm. The collected UV light was transferred through an optical fibre (FC-UV600-0.5-SR, Azpect Photonics) to a spectrometer (grating 2400 grooves/mm, slit width 50 μm, AVABENCH-75-2048, Azpect Photonics). A set of 100 spectra was acquired for each investigated condition and KCl concentrations were evaluated from acquired spectra by a least-squares fit to a calibration spectrum measured at temperature 860 °C following the procedure presented by Forsberg et al. [31].

Measurements of K-atom concentrations were made by tuneable diode laser spectroscopy (TDLAS) using a single-mode external cavity laser (DL 100, Toptica Photonics) with an output power of 40 mW and a central wavelength of 769.9 nm. A scan control module (SC 110) controls a piezoelectric crystal to change the cavity length and obtain wavelength scanning with a repetition rate of 110 Hz. The laser has excellent tuning ability and can be scanned over a frequency range of 25 GHz without mode-hop, and overlaps perfectly with the D_1 line of potassium. The laser beam was guided through the flame at the centre of the burner with a path length of 23 mm. A photodiode detector (DTE 210, Thorlabs) received the laser after absorption by K atoms in the flame. The detector was connected to a data acquisition card (BNC 2110, National Instrument) and an on-line data processing program based on LabVIEW was employed to evaluate K-atom concentrations.

2.2. Burner

A burner originally made for atomic absorption spectroscopy (Perkin-Elmer), shown in the photo of Fig. 1, was used for measurements in alkali-seeded methane-air flames. The burner has a water-cooled head with a central compartment for the premixed fuel-air blend and an outer channel for a co-flow shielding the flame. The diameter of the inner compartment is 23 mm and the head is topped by a circular honeycomb plate (pore size ~1 mm and length 20 mm). The burner allows for stabilization of flat laminar premixed flames (cf. Fig. 1).

Gases are supplied to the burner through a spray chamber with two connections for air, auxiliary air and nebulizer air, and one connection for the fuel. The nebulizer flow provides seeding of alkali solution, which enters via a capillary tube immersed into the liquid. The alkali-solution from the nebulizer is pre-treated as the droplets collide with a so-called impact bead and a flow spoiler in order to have only finer aerosol droplets to pass through the chamber to the burner head while larger droplets are removed via a drain tube. Methane and auxiliary air are mixed together with the nebulizer air in the spray chamber to get the total correct equivalence ratio of the mixture.

A nitrogen co-flow of 10 ln/min was supplied to the burner head to shield the flame. A steel cylinder (cf. Fig. 1) was mounted 30 mm above the burner for flame stabilization required for quantitative signal analysis and to be able to make sequential photofragmentation and Rayleigh scattering measurements under steady-state conditions. The total gas flow of air and fuel to the burner was 5.6 ln/min and individual flows of nitrogen, air to the nebulizer, primary air, and fuel were controlled by four mass flow controllers with maximum flows of 20, 10, 5 and 1 ln/min (Bronkhorst), respectively. Premixed methane-air flames of equivalence ratios Φ = 0.8–1.3 were investigated and the flows of fuel and air are given in Table 1.

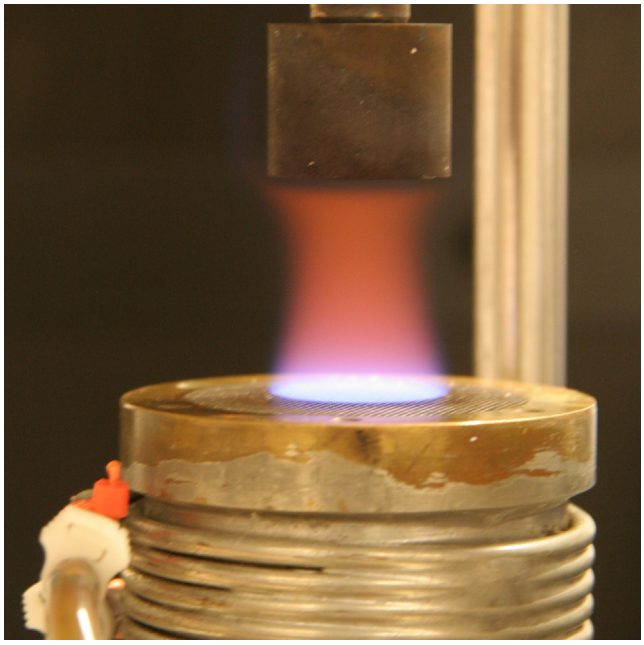

Fig. 1. Methane-air flame of equivalence ratio Φ = 1.1 stabilized on porous plug Perkin-Elmer burner with alkali-seeding (KCl) through a nebulizer. Laminar uniform flames were achieved with a stabilizer mounted 30 mm above the burner surface.

Table 1
Experimental conditions for methane-air flames.

ϕ	CH_4 (L_n/min)	Air (L_n/min)
0.8	0.41	5.19
0.9	0.46	5.14
1	0.51	5.09
1.1	0.55	5.05
1.2	0.60	5.00
1.3	0.64	4.96

2.3. Chemical equilibrium calculations

Post-flame compositions for the investigated flames were obtained through calculations using the PREMIX module in the CHEMKIN software. Conditions of KCl/KOH flame-seeding were then mimicked by introducing atomic species, K and Cl, into the post-flame mixture predicted for each flame. Simulations of these alkali-seeded mixtures were in turn made using the closed homogenous reactor model at temperature 1500 K and atmospheric pressure with a mechanism for alkali-chemistry developed by Hindiyarty et al. [17,32]. These simulations provided concentrations of KCl, KOH, and K atoms versus reaction time and illustrated the progress towards chemical equilibrium for each condition.

3. Results and discussion

3.1. Temperature measurements

Temperatures of the investigated flames were measured by means of Rayleigh scattering and the product gas temperatures for two levels of KCl-seeding are shown in Fig. 2. The temperatures reside within the range 1400–1500 K for both conditions and the uncertainty is estimated to be 9%, indicated by the error bars. Thus, within the estimated accuracy the two data sets provide similar results. The mean temperature value from two data sets show differences up to 70 K and for both conditions the profiles show the same trend versus equivalence ratio with temperature variations less than 50 K. Moreover, the temperatures measured at high KCl-seeding are consistently lower suggesting some cooling by the increased KCl concentration.

3.2. Alkali species concentration measurements

Introducing potassium compounds in the flames result in the formation of atomic potassium as evident from the yellow-red color observed for the seeded flames (cf. Fig. 1). Potassium atom concentrations were measured using TDLAS for seeding of KOH and KCl and the results are shown in Fig. 3. The high absorption cross section of atomic potassium D_1 line, on the order of 10^{-12} cm^2, required rather low seeding concentrations to avoid saturation of the absorption line. Experimental data for seeding with 0.0025 M solution of KOH and 0.005 M solution of KCl are shown in Fig. 3a. While absorption measurements were unattainable at higher seeding levels, the atomic emission lines in the flame chemiluminescence were employed as a measure of the K-atom content in the flame. Fig. 3b shows flame chemiluminescence versus concentration of the KCl solution used for flame seeding. The data plotted in the log-log diagram follow a linear trend with a slope of ½, indicating a dependence on $N^{1/2}$ for the chemilumines-

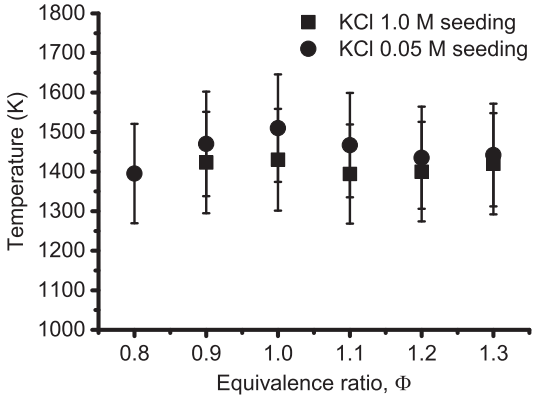

Fig. 2. Average temperature in post-flame region of premixed methane-air flames with two different levels of KCl-seeding to the flame. Circles, 0.05 M solution, squares, 1.0 M solution. The estimated temperature uncertainty is 9% (error bars).

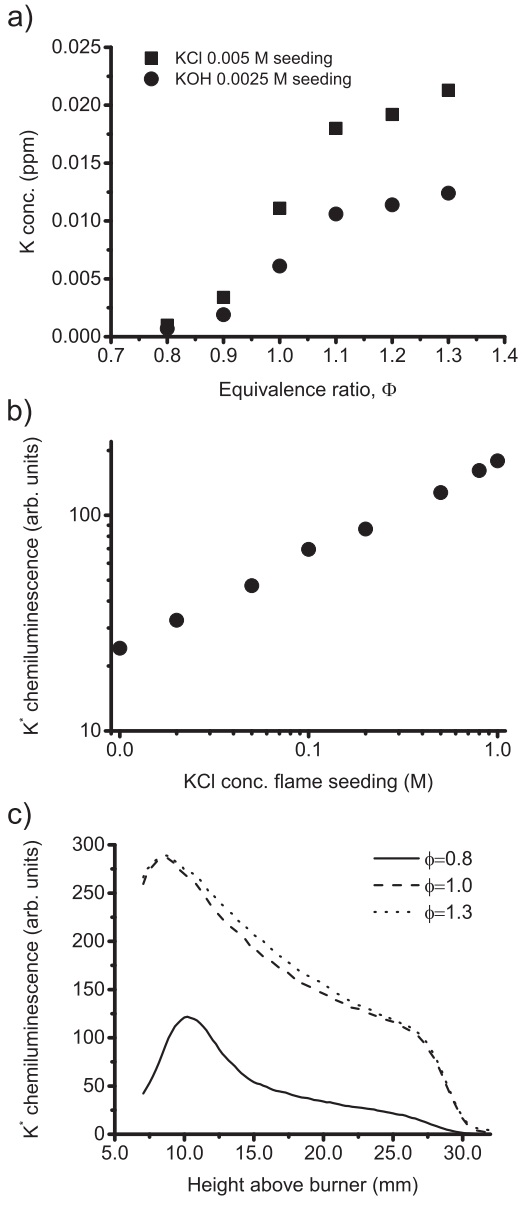

Fig. 3. (a) Post-flame K-atom concentrations versus flame equivalence ratio for seeding of KOH and KCl at solution concentrations 0.0025 and 0.005 M, respectively. (b) K-atom chemiluminescence measured at wavelength 766 nm vs. KCl seeding concentration in the stoichiometric flame. (c) Chemiluminescence profiles measured in lean (Φ = 0.8), stoichiometric, and rich (Φ = 1.3) flame. Higher chemiluminescence signals indicating higher K-atom concentrations are observed for the stoichiometric and fuel-rich flame. The profile of the lean flame shows a more planar shape in the product zone above 12 mm indicating a condition closer to chemical equilibrium compared with the stoichiometric and fuel-rich case.

cence. At high seeding concentrations chemiluminescence is emitted under optically thick conditions where strong absorption at the center of the atomic spectral line result in virtually no transmission of light. However, at the wings of the lineshape absorption is lower allowing for transmission and resulting in the observed $N^{1/2}$ trend. Absorption and emission under optically thick conditions in this type of flames are described more in detail in Refs. [27,28]. This indicates that the K-atom concentration can be considered proportional to the alkali seeding and that concentrations for higher seeding levels can be calculated through extrapolation from the results obtained at low seeding levels by TDLAS and plotted in Fig. 3a.

Fig. 3c shows chemiluminescence versus height above the burner for three different flame stoichiometries and seeding with 1.0 M KCl solution. Peak chemiluminescence positions are located at heights 8–10 mm above the burner and indicate high K-atom levels from the flame-front region. Above these positions the profiles show a rapid decrease up to around 15 mm and then a more gradual decrease with height. A rather uniform temperature profile is expected in the product zone for this type of flame and Rayleigh scattering thermometry indicates temperatures in the range 1300–1500 K (cf. Fig. 2) for the region 11–18 mm above the burner. The observed decrease in chemiluminescence thus probably indicates the progress of K-atom concentrations towards levels corresponding to chemical equilibrium conditions. In the vicinity of the flame stabilizer, mounted 30 mm above the burner, a more rapid decrease attributed to cooling is observed.

The TDLAS results as well as the chemiluminescence profiles show that atomic potassium concentration increase with equivalence ratio, in agreement with observations for sodium in flames burning methane, propane, and hydrogen [8,14]. This can be attributed to increased levels of atomic and molecular hydrogen at fuel-rich conditions. Atomic hydrogen is able to react with potassium hydroxide and/or potassium chloride forming atomic potassium and water or alternatively hydrogen chloride [20]. Equilibrium calculations as outlined above, also predict an increase in K-atom concentration with equivalence ratio and show a trend similar to experiments. Calculations for seeding of 30 ppm KCl into the flame show that the time to establish chemical equilibrium is 8 and 180 ms for the lean $\Phi = 0.8$ and rich $\Phi = 1.3$ flame, respectively. However, the time for transport from the burner surface to the region probed in the TDLAS measurements, around 21 mm above the burner surface, is 19 ms. Thus, while the time to establish chemical equilibrium conditions in the post-flame region of the lean flame is shorter than the transport time, it is longer for the fuel-rich flame and chemical equilibrium is not established, in agreement with the shapes of the chemiluminescence profiles in Fig. 3c.

K-atom concentrations estimated from TDLAS measurements made 21 mm above the burner are 0.2 and 4.4 ppm for the lean and rich flame, respectively. Taking into account transport times and the reaction time profiles obtained from calculations, the K-atom concentrations were calculated to 0.05 and 11 ppm for the lean and rich flame, respectively. As discussed previously, the fuel lean condition is expected to be the closest to chemical equilibrium and the higher experimental value of 0.2 ppm suggests that equilibrium has not been fully established. For the fuel-rich $\Phi = 1.3$ flame, the K-atom concentration from experiments is lower than that predicted by the calculations, suggesting a condition closer to equilibrium with K-atom concentrations of a few ppm. However, it should be noted that calculated K-atom concentrations are rather sensitive to the input temperature. Moreover, some underestimation in experimental K-atom concentrations, obtained from extrapolation of data measured at low seeding, could also be possible even though a linear relation between K-atom concentration and flame seeding is indicated by the results presented in Fig 3b.

Potassium hydroxide and potassium chloride constitute the major alkali compounds formed in the post-flame region when KCl is introduced with the reactants into the flame and the distribution between these compounds depends on the availability of chlorine as well as temperature [20]. Equilibrium calculations as well as analysis of KCl-seeded methane flames presented by Li et al. [17] and simulations by Schofield [20] indicate that low temperature favors chloride formation. Fig. 4 shows alkali compound concentrations measured by UV absorption spectroscopy at flame equivalence ratios $\Phi = 0.8$–1.3. The square symbols represent averages of concentrations evaluated for 100 spectra while the error bars indicate the uncertainty, estimated to 30%, for the absorption measurements in the flames.

Both KCl and KOH show absorption in the wavelength range 230–300 nm probed in the measurements and could contribute to the evaluated absorption spectra. The evaluated concentration thus becomes a sum of the concentrations of the two species. While the peak absorption cross section of KCl at 245 nm has been reported to be $2.0 \cdot 10^{-17}$ cm^2 by Davidovits and Brodhead [33], data for KOH are scarce. However, following the discussion by Sorvajärvi et al. [24] and comparing with values presented for NaOH [34] suggest a KOH absorption cross section of $1.7 \cdot 10^{-17}$ cm^2 at 245 nm. A cross section of KCl on the order of 15% higher than for KOH would result in a correspondingly higher weight for KCl in the sum. However, to take such differences into account require accurate values of the KOH cross section and in the present evaluation cross sections have been assumed to be equal and both species considered to contribute equally to the measured spectrum. With chlorine available at the temperatures of the investigated flames, chemistry is expected to promote KCl formation in the post-flame region, in particular under fuel-rich conditions [20].

Concentrations at lean and stoichiometric conditions are higher than values measured at fuel rich conditions. The observed trend is in agreement with the observed increase in K-atom concentrations with equivalence ratio, cf. Fig. 3a. For comparison with the results from absorption measurements, the sum of the KCl and KOH concentrations, calculated for 30 ppm KCl added to the flame product gas, are also plotted in Fig. 4. The average concentrations measured by absorption spectroscopy drop from 28 ppm at equivalence ratio $\Phi = 0.8$ to typically 15 ppm at fuel-rich conditions. Corresponding values from calculations decrease from 30 to 16 ppm and the trend of the experimental results is thus rather well reproduced by the calculations.

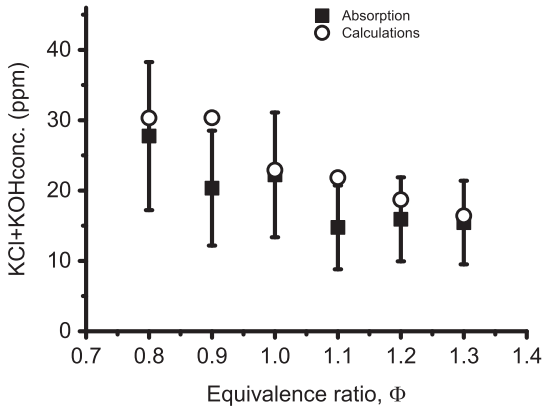

Fig. 4. Post-flame concentrations of potassium compounds measured by UV absorption spectroscopy versus flame equivalence ratio for 1.0 M KCl seeding. Lean conditions show higher KCl concentrations. Square symbols show experimental data while circles represent the sum of calculated KCl and KOH concentrations. Error bars indicate the uncertainty for the UV absorption measurements.

Detection of both KOH and KCl with better sensitivity than the absorption spectroscopy setup is offered by the laser-induced photofragmentation fluorescence technique. However, since both species result in fluorescence emission from K-atom fragments the measured signal contains contributions from both species. Fig. 5 shows alkali compound concentrations measured by photofragmentation fluorescence at flame equivalence ratios $\Phi = 0.8–1.3$ for seeding of KOH (a) and KCl (b) solutions of 0.5 M concentration. For the KOH-seeded flames, without chlorine present, the photofragmentation fluorescence signal only arises from KOH. Since seeding concentrations are the same and atomic potassium levels for both cases are similar (cf. Fig. 3) the sum of KOH and KCl concentrations can be expected to be similar as well. However, the signal obtained for KOH-seeding was a factor of 2.2 lower than for KCl-seeding and this is attributed to differences in the KCl/KOH photofragmentation process. Even though the measurements were made under conditions approaching saturation of the photofragmentation process, for which it is independent on laser irradiance, lower intensity at the temporal wings of the laser pulse will nevertheless generate a signal dependent on irradiance. The relative contribution of this to the total signal will be higher for KOH due to its lower absorption cross section at 193 nm [33,34] resulting in lower photofragmentation efficiency for this species. The energy of the 193 nm laser photons is sufficient for photofragmentation of KCl and generation of K atoms in the $^2P_{1/2}$ and $^2P_{3/2}$ states [22] resulting in fluorescence emission at wavelengths 766.5 and 769.9 nm. However, the lower energy required for dissociation of KOH also allows for formation of K atoms in higher excited states [22] potentially returning to the ground state via transitions not detected in the photofragmentation setup. Due to these effects a lower photofragmentation fluorescence yield can be expected for KOH than for KCl.

For equal concentrations of KCl and KOH in a flame seeded with 0.5 M KCl, a factor of 2.2 higher signal would mean that the KOH photofragmentation fluorescence yield is 30% of the KCl yield. With KCl as the dominant potassium compound, comprising 80% of the total KCl and KOH concentration, the KOH photofragmentation fluorescence yield would instead be 40% of the KCl yield. Using a value of 40% in the evaluation resulted in the KOH concentration profile presented by square symbols in Fig. 5a. The concentrations decrease from 27 to 14 ppm when going from equivalence ratio $\Phi = 0.8$ to $\Phi = 1.3$. Calculated KOH concentrations obtained for an initial concentration of 20 ppm KOH added to the flame product gas are shown with circle symbols in Fig. 5a and decrease from 20 to 5 ppm. The decreasing trend of KOH observed experimentally is thus well reproduced by calculations for the assumed seeding level. Following the discussion above, the evaluated concentration in the KCl-seeded flame is thus expected to represent the concentration of KCl plus 40% of the KOH concentration and the results are presented in Fig. 5b. The concentration evaluated from the photofragmentation fluorescence signal, plotted with square symbols, decreases from 17 ppm at $\Phi = 0.8$ to 10 ppm at $\Phi = 1.3$. A sum of calculated concentrations for KCl and 40% of KOH is plotted with circles in Fig 5b for comparison and drops from 15 to 7 ppm.

Fig. 6 shows alkali compound concentration versus equivalence ratio for 1.0 M (a) and 0.05 M (b) KCl seeding measured by laser-

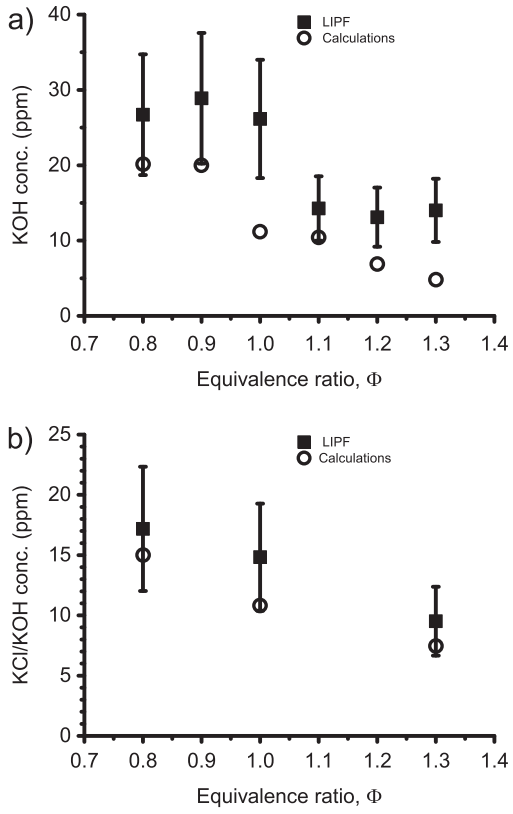

Fig. 5. Post-flame concentration of potassium compounds measured using laser-induced photofragmentation fluorescence (LIPF) versus flame equivalence ratio for seeding of (a) 0.5 M KOH and (b) 0.5 M KCl. Lower KCl/KOH concentrations are measured at fuel-rich conditions due to increased formation of K atoms. Square symbols show experimental data while circles represent results from calculations of potassium species concentrations in flame product gas for (a) KOH and (b) the sum KCl + 40% KOH. The error bars represent the uncertainty of the LIPF data.

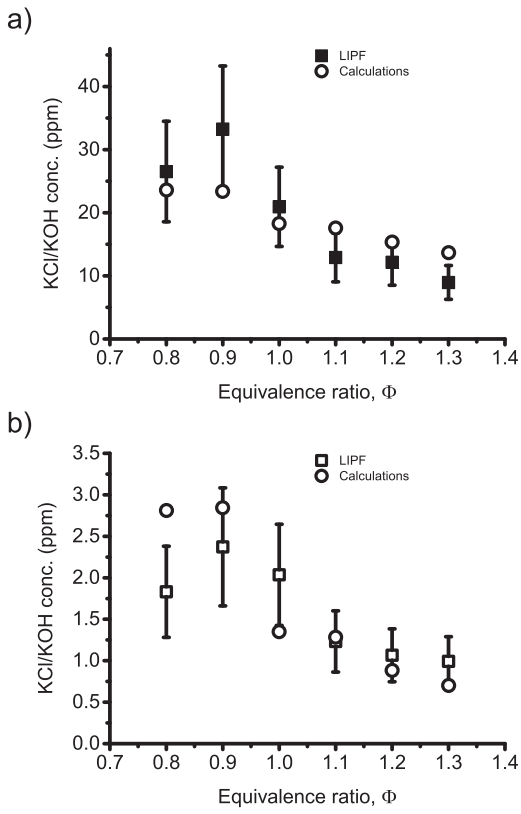

Fig. 6. KCl/KOH concentration measured using laser-induced photofragmentation fluorescence (LIPF) versus flame equivalence ratio for seeding with different potassium and chlorine levels. (a) 1.0 M KCl seeding (b) 0.05 M KCl seeding. Lower KCl/KOH concentrations are obtained under fuel-rich conditions. Square symbols show experimental data while circles represent calculated potassium species concentrations in the flame product gas, the sum KCl+40% KOH in (a) and KOH in (b). The error bars represent the uncertainty of the LIPF data.

induced photofragmentation fluorescence. Following the previous discussion related to Fig. 4 and 5, the case of high KCl-seeding is expected to give higher concentrations of KCl than KOH. In that case KCl forms the main contribution to the photofragmentation fluorescence signal and the evaluated concentration mainly represents KCl. Seeding with 1.0 M KCl solution, cf. Fig. 6a, results in post-flame concentrations up to 33 ppm at lean conditions decreasing to 21 ppm at $\Phi = 1.0$ and 9 ppm at $\Phi = 1.3$. The sum of KCl and 40% of the KOH concentration, obtained by calculations for 30 ppm of KCl added to the flame product gas, decreases from 24 to 14 ppm.

Better overall agreement between experiments and simulations were obtained for the absorption data presented in Fig. 4. At equivalence ratios $\Phi = 0.8$ and $\Phi = 1.0$, photofragmentation data show good agreement with calculations whereas the experimental value obtained for $\Phi = 0.9$ is higher than the calculated concentration. At fuel-rich conditions, experimental concentrations are consistently lower than results from calculations, indicating that the experimental conditions are further from chemical equilibrium condition than the calculations predict.

At 0.05 M KCl-seeding, resulting in chlorine levels of a few ppm, equilibrium calculations as well as previous flame studies indicate KOH to be the dominant post-flame potassium compound. For example, simulations of hydrogen and propane flames seeded with sodium chloride, presented by Schofield [14], indicate negligible amounts of alkali chloride compared with hydroxide and atom levels at chlorine concentrations below 10 ppm. Thus, data measured at this seeding level can be expected to mainly represent KOH. Photofragmentation data measured for 0.05 M KCl-seeding, presented in Fig. 6b, also show a decrease in alkali compound concentration with equivalence ratio from 1.8 to 1.0 ppm. For the 0.05 M solution seeding, experimental conditions were mimicked by calculations for 4 ppm KCl seeded to the flame product gas. The KOH concentration obtained by calculations decreases from 2.8 to 0.7 ppm.

3.3. Alkali balance

Since free K atoms together with KCl and KOH constitute the major potassium species in the post-flame region, conservation of K atoms implies that the sum of the concentrations of these species should be constant. The concentration balances of these species for the investigated flames are presented in Fig. 7. Fig. 7a presents a bar chart with concentrations of K and KCl/KOH measured in flames for 1.0 M KCl seeding. K-atom concentrations calculated by extrapolation of TDLAS results are presented with black bars and KCl/KOH concentrations are presented with grey bars on top of the black ones. The height of the total bar thus represents the sum of the concentrations. Concentrations of KCl/KOH are presented both with the results from absorption measurements (dark grey bars) and laser-induced photofragmentation fluorescence (light grey bars) together with corresponding error bars representing the experimental uncertainty.

Absorption and laser-induced photofragmentation fluorescence data show a decrease of 13 and 18 ppm in KCl/KOH concentration, respectively between equivalence ratios $\Phi = 0.8$ and $\Phi = 1.3$. These results are not fully counterbalanced by the increase in K-atom concentrations obtained from TDLAS data. A possible reason for this could be an uncertainty in the contribution from KOH to the evaluated concentrations, assumed to represent sums of KCl and KOH. For example, an underestimation of the KOH absorption cross section by 10–20%, would give KOH concentrations overestimated by 2–6 ppm, which could partially account for the observed difference in total alkali concentrations when going from lean to fuel-rich conditions. As discussed previously, concentrations evaluated from laser-induced photofragmentation fluorescence data only

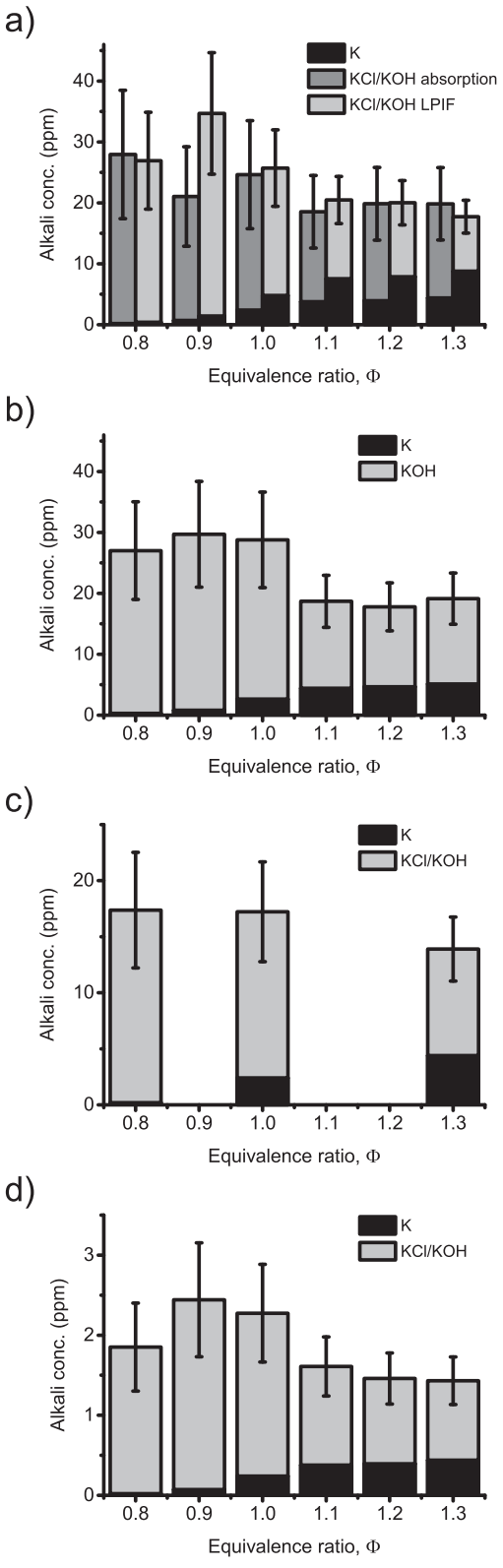

Fig. 7. Bar charts illustrating balance of alkali species concentrations for the investigated flames. The sum of K-atom concentrations (black bars) and KCl/KOH concentrations (grey bars) is constant within the experimental uncertainties indicated by the error bars. (a) 1.0 M KCl seeding, (b) 0.5 M KOH seeding, (c) 0.5 M KCl seeding, and (d) 0.05 M KCl seeding. KCl/KOH concentration measured by laser-induced photofragmentation fluorescence are presented with light grey bars for all the flames. For the 1.0 M flame presented in (a), KCl/KOH concentrations were also measured by absorption spectroscopy and these values are presented with dark grey bars.

partially include the contribution for KOH, which could result in an underestimation on the order of 5 ppm.

The TDLAS data give K-atom concentrations increasing from 0.2 to 4.4 ppm, however, an underestimation, as discussed previously, could also be a possible explanation for the observed difference. In addition, this could account for the difference compared with calculations, predicting an increase from 0.1 to 12 ppm. The K-atom concentrations were measured at a similar height as the UV absorption measurements 20 mm above the burner, this position is, however, located higher than the evaluation region of photofragmentation fluorescence,~12–18 mm above the burner surface. Chemiluminescence profiles (cf. Fig. 3c) suggest K-atom levels in this region to be up to a factor of two higher than values obtained from the TDLAS data. Considering this, K-atom concentrations for comparison with the LIPF data would increase from 0.4 to 9 ppm between equivalence ratios $\Phi = 0.8$ and $\Phi = 1.3$. For comparison, calculations for these conditions give K-atom concentrations increasing from 0.1 ppm to 14 ppm. The increase in experimental K-atom concentrations would then approach the decrease in KCl/KOH concentrations. Altogether, the difference between the trends for KCl/KOH and K atoms is still within the uncertainty and spread of the experimental data, indicated by error bars in Fig. 7a, and the total concentration of potassium species is conserved.

The potassium balance for the flame seeded with 0.5 M KOH solution is shown in Fig. 7b with KOH concentrations decreasing from 27 to 14 ppm while the K-atom concentrations increase from 0.3 to 5 ppm. However, considering the estimated KOH measurement accuracy, indicated by the error bars in Fig. 7b, the decrease could be smaller and the potassium species concentrations remain balanced. The result for 0.5 M KCl seeding is shown in Fig. 7c with K-atom concentrations increasing from 0.2 to 4.4 ppm and KCl/KOH concentrations decreasing from 17 to 10 ppm. Within the experimental uncertainties of the photofragmentation data, the decrease in KCl/KOH concentrations is in agreement with the increase in K-atom concentrations. For comparison, calculations give an increase in K-atom concentrations from 0.1 to 9 ppm.

The results for the flames seeded with 0.05 M KCl solution are shown in Fig. 7d and KCl/KOH concentrations show a 0.8 ppm decrease from 1.8 to 1.0 ppm. K-atom concentrations derived from experimental data increase from 0.002 to 0.4 ppm, cf. Fig. 3a and c, while calculations result in an increase from 0.02 to 3 ppm. Also in this case the sum of potassium species concentrations is constant within the estimated experimental uncertainties indicated by the error bars.

The accuracy of the methods employed for species concentrations is dependent on experimental conditions and knowledge on relevant quantities. Accurate absorption measurements require homogeneous distribution of the measured species along the light path as well as knowledge on path length and absorption cross sections. Homogenous alkali species distributions can be obtained in the investigated one-dimensional flames and the path length can be determined rather accurately from visualization of alkali species distributions using the photofragmentation fluorescence imaging. For K atoms, absorption cross sections are fairly well known making TDLAS a robust and reliable technique. For alkali compounds KCl and KOH less information is available. A cell for calibration of KCl absorption measurements and determination of UV absorption cross section at temperatures relevant for KCl in combustion flue gas has, however, been presented recently [35]. For KOH, data is unfortunately lacking and the presented analysis relies on estimations, as discussed previously. In addition, methods for refined analysis of UV absorption spectra would clearly be beneficial for improved distinction between KCl and KOH.

The accuracy of the photofragmentation data is dependent on the uncertainties of the quantities in Eq. (1). This includes uncertainties in the calibration versus Rayleigh scattering, the laser sheet cross section area, the collisional quenching factor, the trapping factor, and the photofragmentation fluorescence yield of KOH. For a set of measurements at different equivalence ratios the signal calibration, the laser sheet area, and the KOH yield remain constant and uncertainties in their values would introduce constant over- or underestimation in evaluated concentrations for the entire set. The uncertainty for the Rayleigh scattering measurement used for signal calibration is mainly attributed to the laser pulse energy, which can be determined with an accuracy on the order of 5%. By comparison with concentrations evaluated from UV absorption measurements at high KCl-seeding, the uncertainty in the width of the focused laser sheet has been estimated to 20%. The KOH yield, as discussed previously, is a factor between 0.3 and 0.4 of the KCl yield and an uncertainty in this factor by 0.05 corresponds to an uncertainty in the yield of 15%. The collisional quenching and trapping factor depend on flame conditions and vary with equivalence ratio. The uncertainty in temperature (cf. Fig. 2) equivalence ratios introduces an uncertainty of 5% in the collisional quenching rate. The fluorescence trapping is dependent on the K-atom concentration and variations of 15%, corresponding to the spread in the values of a TDLAS data point in Fig. 3, result in a change in the trapping factor by 8%. In addition, multiple averaged photofragmentation fluorescence images show a variation in signal strength by 2%, representing uncertainties introduced by the detection system and possible variations in the flame. Combining these uncertainties have resulted in an overall uncertainty for the photofragmentation fluorescence data of 30%.

For all cases presented above, the K-atom concentrations predicted by calculations are higher than values retrieved from experimental data. This could imply that the chemistry has progressed further towards equilibrium conditions, resulting in lower K-atom concentrations, than predicted by the calculations. However, it should be noted that calculations are made for a constant temperature and that calculated K-atom concentrations are rather sensitive to the input temperature. Higher temperature favors atomic species formation and result in higher equilibrium concentrations, which is exemplified by results obtained for sodium-seeded propane flames by Schofield [20]. In simulations of those flames, temperatures were around 2000 K and atomic sodium constituted around 10% or less of the total alkali content at equivalence ratio $\Phi = 0.8$. At a fuel rich $\Phi = 1.2$ condition, the Na atom instead represented around 80% of the total alkali content. For flames investigated in this study, measured temperatures were 1400–1500 K and for the lean flame of 1.0 M KCl seeding, the K-atom concentration of 0.02 ppm corresponds to on the order of 0.05% of the total alkali content while the 4.4 ppm obtained at equivalence ratio $\Phi = 1.3$ corresponds to 12%.

Altogether, for flame-seeding with KOH as well as KCl, alkali-compound levels decrease with increasing flame equivalence ratio whereas atomic potassium shows an opposite trend. As mentioned previously, similar observations have been made for sodium species concentrations in premixed sodium-seeded propane and hydrogen flames [20]. The observed trend is also in good agreement with predictions from calculations. While the transport times are sufficient for establishing equilibrium conditions in the lean flames this is likely not the case for the stoichiometric and fuel-rich conditions. Nevertheless, also for chemical equilibrium calculations show lower concentrations of KCl and KOH and correspondingly higher concentrations of K atoms under fuel-rich conditions.

4. Conclusions

Alkali species concentrations obtained from non-intrusive optical measurements in potassium-seeded premixed methane-air

flames have been compared with results from calculations using a mechanism for potassium chemistry in a homogeneous reactor model. Experimental results show agreement within estimated uncertainties with predictions from the model calculating concentrations in the post-flame region. The burner and diagnostic methods employed thus present a suitable experimental configuration for further detailed studies for validation and development of alkali combustion chemistry models. The combination enables investigations under well-defined experimental conditions arranged to obtain information relevant for biofuel combustion. Such investigations provide insights necessary for understanding of combustion also at larger scales. For example, on specific phenomena related to alkali in combustion, such as sulfation for abatement of deposit formation and catalytic effects.

Acknowledgements

The authors appreciate financial support from the Swedish Energy Agency, the Knut and Alice Wallenberg foundation [grant number KAW 2015.0294], ERC advanced grant TUCLA [grant number 669466], and Vattenfall AB. The helpful discussions and long-term fruitful collaboration with Professor Peter Glarborg and Assistant Professor Hao Wu at Denmark Technical University, through the GREEN project supported by the Danish Council for Strategic Research, are gratefully acknowledged.

Appendix A. Supplementary data

Supplementary data associated with this article can be found, in the online version, at http://dx.doi.org/10.1016/j.fuel.2017.05.013.

References

[1] Abbasi T, Abbasi SA. Biomass energy and the environmental impacts associated with its production and utilization. Renew Sust Energ Rev 2010;14:919–37.
[2] Khan AA, de Jong W, Jansens PJ, Spliethoff H. Biomass combustion in fluidized bed boilers: potential problems and remedies. Fuel Process Technol 2009;90:21–50.
[3] Knudsen JN, Jensen PA, Dam-Johansen K. Transformation and release to the gas phase of Cl, K, and S during combustion of annual biomass. Energ Fuel 2004;18:1385–99.
[4] Johansen JM, Jakobsen JG, Frandsen FJ, Glarborg P. Release of K, Cl, and S during pyrolysis and combustion of high-chlorine biomass. Energ Fuel 2011;25:4961–71.
[5] Vassilev SV, Baxter D, Vassileva CG. An overview of the behaviour of biomass during combustion: Part I. Phase-mineral transformations of organic and inorganic matter. Fuel 2013;112:391–449.
[6] Nunes LJR, Matias JCO, Catalao JPS. Biomass combustion systems: a review on the physical and chemical properties of the ashes. Renew Sust Energ Rev 2016;53:235–42.
[7] Antunes RA, de Oliveira MCL. Corrosion in biomass combustion: a materials selection analysis and its interaction with corrosion mechanisms and mitigation strategies. Corros Sci 2013;76:6–26.
[8] van Loo S, Koppejan J. The handbook of biomass combustion and co-firing. London: Earthscan; 2008.
[9] Glarborg P. Hidden interactions – Trace species governing combustion and emissions. Proc Combust Inst 2007;31:77–98.
[10] Kassman H, Pettersson J, Steenari BM, Åmand LE. Two strategies to reduce gaseous KCl and chlorine in deposits during biomass combustion - injection of ammonium sulphate and co-combustion with peat. Fuel Process Technol 2013;105:170–80.
[11] Madanayake BN, Gan SY, Eastwick C, Ng HK. Biomass as an energy source in coal co-firing and its feasibility enhancement via pre-treatment techniques. Fuel Process Technol 2017;159:287–305.
[12] Abuelnuor AAA et al. Characteristics of biomass in flameless combustion: a review. Renew Sust Energ Rev 2014;33:363–70.
[13] Ekvall T, Andersson K, Leffler T, Berg M. K-Cl-S chemistry in air and oxy-combustion atmospheres. P Combust Inst 2017;36:4011–8.
[14] Hynes AJ, Steinberg M, Schofield K. The chemical-kinetics and thermodynamics of sodium species in oxygen-rich hydrogen flames. J Chem Phys 1984;80:2585–97.
[15] Rosser WA, Inami SH, Wise H. The effect of metal salts on premixed hydrocarbon air flames. Combust Flame 1963;7:107–19.
[16] Slack M, Cox JW, Grillo A, Ryan R, Smith O. Potassium kinetics in heavily seeded atmospheric-pressure laminar methane flames. Combust Flame 1989;77:311–20.
[17] Li B et al. Post-flame gas-phase sulfation of potassium chloride. Combust Flame 2013;160:959–69.
[18] Li WQ et al. Effect of atmosphere on the release behavior of alkali and alkaline earth metals during coal oxy-fuel combustion. Fuel 2015;139:164–70.
[19] Mason PE, Darvell LI, Jones JM, Williams A. Observations on the release of gas-phase potassium during the combustion of single particles of biomass. Fuel 2016;182:110–7.
[20] Schofield K. The chemical nature of combustion deposition and corrosion: the case of alkali chlorides. Combust Flame 2012;159:1987–96.
[21] Monkhouse P. On-line spectroscopic and spectrometric methods for the determination of metal species in industrial processes. Prog Energ Combust 2011;37:125–71.
[22] Oldenborg RC, Baughcum SL. Photofragment fluorescence as an analytical technique – application to gas-phase alkali chlorides. Anal Chem 1986;58:1430–6.
[23] Qu ZC, Steinvall E, Ghorbani R, Schmidt FM. Tunable diode laser atomic absorption spectroscopy for detection of potassium under optically thick conditions. Anal Chem 2016;88:3754–60.
[24] Sorvajärvi T, DeMartini N, Rossi J, Toivonen J. In situ measurement technique for simultaneous detection of K, KCl, and KOH vapors released during combustion of solid biomass fuel in a single particle reactor. Appl Spectrosc 2014;68:179–84.
[25] Leffler T, Brackmann C, Aldén M, Li ZS. Laser-induced photofragmentation fluorescence imaging of alkali compounds in flames. Appl Spectrosc 2016 (accepted for publication).
[26] Sansonetti JE. Wavelengths, transition probabilities, and energy levels for the spectra of potassium (K I through K XIX). J Phys Chem Ref Data 2008;37:7–96.
[27] Alkemade CTJ, Herrmann R. Fundamentals of analytical flame spectroscopy, Bristol. UK: Adam Hilger Ltd.; 1979.
[28] van Trigt C, Hollander TJ, Alkemade CTJ. Determination of the a′-parameter of resonance lines in flames. J Quant Spectrosc Radiat Transfer 1965;5:813–33.
[29] Jenkins DR. Determination of cross sections for quenching of resonance radiation of metal atoms. 2. Results for potassium rubidium and caesium. Proc R Soc Lon Ser-A 1968;303:453–65.
[30] Zetterberg J, Development of laser-spectroscopi techniques for new detection schemes in combustion diagnostics, Department of Physics/Combustion Physics, Lund University, 2008.
[31] Forsberg C et al. Principle, calibration, and application of the in situ alkali chloride monitor. Rev Sci Instrum 2009;80.
[32] Hindiyarti L, Frandsen F, Livbjerg H, Glarborg P, Marshall P. An exploratory study of alkali sulfate aerosol formation during biomass combustion. Fuel 2008;87:1591–600.
[33] Davidovits P, Brodhead DC. Ultraviolet absorption cross sections for alkali halide vapors. J Chem Phys 1967;46:2968–73.
[34] Self DE, Plane JMC. Absolute photolysis cross-sections for $NaHCO_3$, NaOH, NaO, NaO_2 and NaO_3: implications for sodium chemistry in the upper mesosphere. Phys Chem Chem Phys 2002;4:16–23.
[35] Leffler T, Brackmann C, Berg M, Aldén M, Li ZS. Development of an alkali chloride vapour-generating apparatus for calibration of ultraviolet absorption measurements. Rev Sci Instrum 2017;88.